Neural Mechanisms for Generating Rate and Temporal Codes in Model CA3 Pyramidal Cells

VICTORIA BOOTH AND AMITABHA BOSE

Department of Mathematical Sciences, Center for Applied Mathematics and Statistics, New Jersey Institute of Technology, Newark, New Jersey 07102-1982

Received 18 September 2000; accepted in final form 14 February 2001

Booth, Victoria and Amitabha Bose. Neural mechanisms for generating rate and temporal codes in model CA3 pyramidal cells. *J Neurophysiol* 85: 2432–2445, 2001. The effect of synaptic inhibition on burst firing of a two-compartment model of a CA3 pyramidal cell is considered. We show that, depending on its timing, a short dose of fast decaying synaptic inhibition can either delay or advance the timing of firing of subsequent bursts. Moreover, increasing the strength of the inhibitory input is shown to modulate the burst profile from a full complex burst, to a burst with multiple spikes, to single spikes. We additionally show how slowly decaying inhibitory input can be used to synchronize a network of pyramidal cells. Implications for the phase precession phenomenon of hippocampal place cells and for the generation of temporal and rate codes are discussed.

INTRODUCTION

Place cells in region CA3 of rat hippocampus have been observed to fire in a spatially specific and a temporally specific manner. As the rat enters a place field, the corresponding place cell, generally considered to be a pyramidal cell, commences firing (O'Keefe and Dostrovsky 1971), and a change in firing rate has been observed as the place field is crossed. Two experimental studies observed an increase in the firing rate as the center of the field was approached and then a decrease as the field was exited (O'Keefe and Recce 1993; Skaggs et al. 1996). This firing rate change has been modeled as a two-dimensional Gaussian function of the animal's Cartesian location in the environment (O'Keefe and Burgess 1996). In a study of CA1 pyramidal cells, a more monotonic increase in firing rate was observed with lowest firing rate at the beginning of the place field and highest rate at the end (Mehta et al. 2000). The preferential firing of place cells in place fields suggests a firing rate code for location, and the observed changes in firing rate as the field is crossed may code for location within the field. A specific relationship between timing of place cell firing and the hippocampal electroencephalogram (EEG), or theta rhythm, has also been observed as a rat runs along a linear runway. Namely, the phase of the theta rhythm at which a place cell fires systematically precesses as the place field is crossed (O'Keefe and Recce 1993; Skaggs et al. 1996). Each time the animal enters the place field, firing begins at the same phase, and over the next 5 to 10 cycles of the theta rhythm it undergoes up to 360° of phase precession. These findings suggest that there may also be a temporal code for location in the phase of firing relative to the theta rhythm. It has recently been shown that a rat's location can be more accurately predicted when both rate and phase information are taken into account (Jensen and Lisman 2000).

Despite the fact that much of the hippocampal anatomy is known, the neural mechanisms generating the changes in firing rate as the place field is crossed and the phenomenon of phase precession have not been completely determined. Place cells are known to receive excitatory synaptic projections from dentate granule cells (Claiborne et al. 1986) as well as cholinergic excitation from the medial septum (Shute and Lewis 1963). They also receive synaptic inhibition from a variety of interneurons (Freund and Buzsáki 1996) that are influenced by GABAergic projections from the medial septum (Freund and Buzsáki 1996). In addition, place cells project to interneurons (Csicsvari et al. 1998) offering the possibility of feedback inhibition after place cell firing (Karnup and Stelzer 1999). The theta rhythm may further modulate place cell firing (Kamondi et al. 1998).

Several models to account for place cell firing patterns have been proposed (Bose et al. 2000; Jensen and Lisman 1996; Kamondi et al. 1998; Tsodyks et al. 1996; Wallenstein and Hasselmo 1997). In some of these models, the phase of place cell firing within the place field is essentially environment driven with precession occurring as a result of recall of stored memories for neighboring locations (Jensen and Lisman 1996; Tsodyks et al. 1996; Wallenstein and Hasselmo 1997). Alternatively, phase precession has been achieved by varying the total amount of depolarization to the cell (Kamondi et al. 1998). The models that address the firing rate changes within a place field rely on increasing depolarization to the cell as the place field is crossed to achieve the observed rate pattern (Kamondi et al. 1998; Tsodyks et al. 1996). We have previously proposed a minimal CA3 network model (Bose et al. 2000) that uses synaptic inhibition to control the timing of place cell firing and generate the onset, occurrence, and end of phase precession. As only the burst envelope of place cell firing was modeled, mechanisms to account for the changes in firing rate as the place field is crossed were not addressed.

It has been shown both in experiment and in models that inhibitory input to pyramidal cells can alter their firing pattern. In CA3 pyramidal cells in vitro (Traub et al. 1994) and in multicompartmental models (Kepecs and Wang 2000; Traub et

Address reprint requests to V. Booth (E-mail: vbooth@m.njit.edu).

The costs of publication of this article were defrayed in part by the payment of page charges. The article must therefore be hereby marked "*advertisement*" in accordance with 18 U.S.C. Section 1734 solely to indicate this fact.

al. 1994), inhibition arriving at dendritic locations could suppress the onset of bursting. It was additionally observed in the model, that dendritic inhibition, when timed appropriately, truncated the somatic burst envelope (Traub et al. 1994). In these pyramidal cells, complex burst firing depends on a dendritic Ca^{2+}-based depolarization supporting sodium action potentials initiated closer to the soma. Usually these complex bursts are initiated by leading sodium spikes that back-propagate to trigger the dendritic depolarization. Traub et al. (1994) surmised that the effects of inhibition on burst waveform were a result of suppression of dendritic Ca^{2+}-based depolarization. Suppression of dendritic Ca^{2+}-based spikes by synaptic inhibition was observed in dendritic recordings of hippocampal pyramidal cells in vitro (Miles et al. 1996; Tsubokawa and Ross 1996) and in vivo (Buzsáki et al. 1996). Furthermore, depending on the strength and timing of the inhibition, relative to leading sodium spikes, inhibition could delay the activation of the dendritic Ca^{2+}-based spike, or it could abort an already activated spike (Buzsáki et al. 1996). While in some of these studies, suppression of the calcium spike resulted in no observed change in somatic firing (Tsubokawa and Ross 1996), in cortical pyramidal cells, when the dendritic calcium spike was inhibited, the associated action potential burst was completely abolished (Larkum et al. 1999). In a modeling study of a CA3 pyramidal neuron, dendritic inhibition could modulate somatic firing in a more graded manner (Kepecs and Wang 2000).

In this paper, we investigate the effects of synaptic inhibition on burst firing of a model CA3 pyramidal cell. We consider a two-compartment model, developed by Pinsky and Rinzel (1994, 1995), synaptically coupled to an excitable interneuron. We find that synaptic inhibition can advance or delay the timing of burst firing with the timing of inhibition determining the effect. As a result, periodically timed inhibition can alter the frequency of burst firing, acting to increase or decrease it in a range around the intrinsic burst frequency. Furthermore, we find that, depending on its strength, inhibition can modulate calcium influx into the dendrites, such that the cell will fire full complex bursts, bursts with a small number of spikes, or single spikes. This results in a mapping between synaptic weight, firing frequency, and burst waveforms.

While the two-compartment model has sufficient detail to generate complex bursts with compartmentally segregated mechanisms (Pinsky and Rinzel 1994) (and see *Model*), we take advantage of its relative simplicity to analyze the effects of inhibition on burst firing using phase plane methods. A result of this analysis is a new insight into the mechanisms underlying complex burst generation. Briefly, in a repetitively bursting neuron, we find that burst initiation does not strictly depend on dendritic mechanisms but depends more on the interaction between somatic and dendritic voltages. Dendritic inhibition has the effect of decoupling these two influences to reveal the distinction. We also find that, when inhibition modulates the dendritic active response, the interaction between somatic and dendritic voltage, sometimes referred to as soma-dendritic "ping-pong" (Wang 1999), plays a crucial role in determining burst waveform.

Using the results of synaptic inhibition on a single pyramidal cell, we additionally investigate the effects of inhibition on anatomically isolated or weakly connected pyramidal cells. Previous modeling studies have shown that a network of pyramidal cells with fast, recurrent excitatory synapses display synchronous oscillations (Pinsky and Rinzel 1994; Traub et al. 1993). We show that synaptic inhibition is an alternate mechanism for synchronizing a network of pyramidal cells, as has been demonstrated in vitro in the CA1 region by Cobb et al. (1995). Moreover, we show that bistability can be obtained between synchronous and out-of-phase network rhythms.

MODEL AND METHODS

Model

The CA3 pyramidal cell model developed by Pinsky and Rinzel (1994, 1995) consists of a soma compartment electrotonically coupled to a dendrite compartment. The soma compartment contains a fast, inactivating sodium current and a potassium delayed-rectifier current and, when isolated from the dendrite compartment, repetitively fires action potentials at a range of frequencies (from very low up to 300 Hz) in response to maintained applied current I_s. The dendrite compartment contains a calcium current and two potassium currents. A slowly activating afterhyperpolarization (AHP) current has gating variable q that depends only on Ca^{2+} concentration. The other potassium current is fast activating with activation depending on voltage, but the conductance also contains a saturating term that depends on Ca^{2+} concentration. When isolated from the soma, the dendrite compartment generates low-frequency Ca^{2+}-based spikes. When the compartments are coupled together electrotonically, the model displays a variety of firing patterns in response to somatic applied current or dendritic synaptic input, including very low-frequency bursting (less than 8 Hz), low-frequency bursting (8–20 Hz), and fast, periodic spiking (30 Hz). Bursting occurs in the model due to interactions between the soma and dendrite compartments in what has been dubbed soma-dendritic "ping-pong" (Wang 1999). Specifically, a burst is initiated by a somatic sodium spike that triggers a dendritic calcium spike. Successive somatic spikes in the burst are caused by depolarization of the soma by the slower dendritic calcium spike. The burst ends when the dendritic calcium spike ends. The burst profile is not uniform but is characterized by an interval of high-frequency, damped spiking in the middle due to the large dendritic depolarization during the calcium spike overdriving the somatic spike generator. We consider the model in the very low-frequency bursting regime with somatic applied current $I_s = 0.5$ ($\mu A/cm^2$). With this low level of stimulation, the model displays periodic bursting at approximately 1.5 Hz.

We synaptically couple this pyramidal cell to an excitable interneuron (Fig. 1) that generates an action potential in response to a brief applied current pulse or synaptic excitation. The interneuron is modeled with the Morris-Lecar equations (Morris and Lecar 1981). We consider two synaptic architectures in this two-cell network. In the first network structure, the only synaptic connection is between the interneuron and the pyramidal cell with fast inhibitory synaptic current arriving to the dendrite compartment. With this network, we consider the effect of inhibition arriving during the interburst interval. In the second network structure, in addition to the connection between interneuron and dendrite compartment, the soma compartment of the pyramidal cell makes a fast excitatory synaptic connection back onto the interneuron. With this network structure, where the pyramidal cell receives feedback inhibition from the interneuron, we consider the effects of inhibition arriving during a burst. We do not include a synaptic delay in either connection.

The equations for this two cell network are

$$C_m V_s' = -I_{Na}(V_s, h) - I_{K-DR}(V_s, n) - I_{Leak}(V_s) + I_s/p + g_c(V_d - V_s)/p$$

$$C_m V_d' = -I_{Ca}(V_d, s) - I_{K-C}(V_d, c, Ca) - I_{K-AHP}(V_d, q) - I_{Leak}(V_d) + g_c(V_s - V_d)/(1-p) - g_{\text{inh}} s_{\text{inh}}(V_d - V_{\text{inh}})$$

$$C_m V_i' = -I_{Ca}(V_i) - I_K(V_i, w) - I_L(V_i) + I_i - g_{\text{exc}} s_{\text{exc}}(V_i - V_{\text{exc}})$$

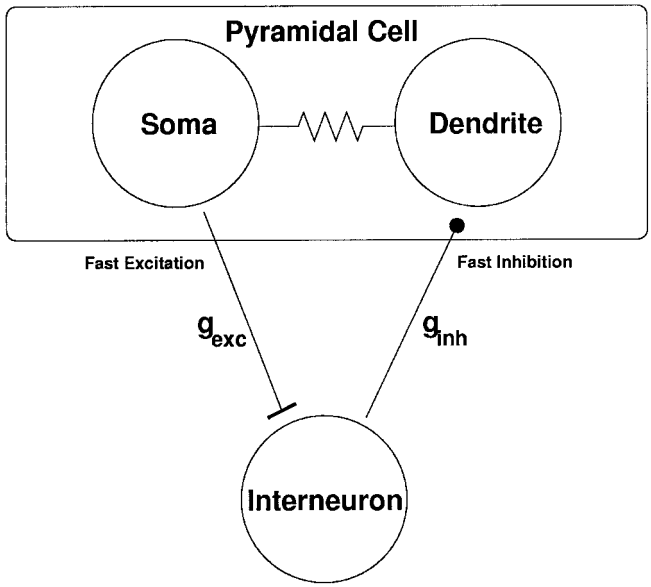

FIG. 1. Pinsky-Rinzel (1994) 2-compartment CA3 pyramidal cell synaptically coupled to an excitable interneuron. Inhibitory (excitatory) synaptic current from interneuron (soma compartment of pyramidal cell) to dendrite compartment of pyramidal cell (interneuron) controlled by maximal conductance g_{inh} (g_{exc}).

where V_s, V_d, and V_i are voltages in the soma and dendrite compartments and the interneuron, respectively. We refer the reader to the original references of the pyramidal cell model for the ionic current terms, gating equations, intracellular calcium equation, and parameter values (Pinsky and Rinzel 1994, 1995). In our phase plane analysis, however, we will refer specifically to the gating variables n (for the somatic, delayed-rectifier current) and q (for the dendritic, slow AHP current), and to the intracellular calcium concentration in the dendrite, Ca. The parameter g_c is the coupling conductance between compartments, and p represents the fraction of the total area of the cell occupied by the soma compartment. The ionic current terms for the interneuron are $I_{Ca}(V_i) = g_{Ca}m_\infty(V_i)(V_i - V_{Ca})$, $I_K(V_i, w) = g_K w(V_i - V_K)$ and $I_L(V_i) = g_L(V_i - V_L)$. The gating equation for w is $w' = 0.08[w_\infty(V_i) - w]/\tau_w(V_i)$. The steady-state activation functions are $m_\infty(V_i) = 0.5\{1 + \tanh[(V_i + 1.2)/18]\}$ and $w_\infty(V_i) = 0.5\{1 + \tanh[(V_i + 25)/11]\}$. The time constant function is $\tau_w(V_i) = 1/\cosh[(V_i + 25)/22]$. The maximal conductances (in mS/cm^2) are $g_{Ca} = 4.4$, $g_K = 8$, $g_L = 2$. The reversal potentials (in mV) are $V_{Ca} = 120$, $V_K = -84$ and $V_L = -60$. Membrane capacitance is $C_m = 3\ \mu$F/cm^2. The applied current to the interneuron is $I_i = 88\ \mu$A/cm^2, which assures that the interneuron is excitable.

The strength of synaptic current is governed by a maximal conductance g_{inh} for the synapse from interneuron to pyramidal cell and g_{exc} for the synapse from pyramidal cell to interneuron. In the first synaptic architecture we consider, g_{exc} is set to zero, then it is made nonzero for the second network structure (see figure captions for values). The reversal potential in the synaptic current terms determines whether the synapse is excitatory or inhibitory; we set $V_{\text{inh}} = -80$ mV and $V_{\text{exc}} = 0$ mV. The dynamics of the synaptic currents are governed by equations of the form

$$s'_{\text{inh/exc}} = \alpha H_\infty(V_x - V_{\text{thresh}})(1 - s_{\text{inh/exc}}) - \beta H_\infty(V_{\text{thresh}} - V_x)s_{\text{inh/exc}}$$

where V_x is presynaptic voltage. The Heaviside function, H_∞, is used to enforce the synaptic threshold. The constants $\alpha = 2$ mS^{-1} and $\beta = 1$ mS^{-1} are the rise and decay rates, respectively, of the synapse, and $V_{\text{thresh}} = -10$ mV is the synaptic activation threshold. We work primarily in the regime where the synaptic currents are fast acting and decaying, meant to mimic α-amino-3-hydroxy-5-methyl-4-isoxazolepropionic acid (AMPA)–mediated excitation and GABA-A–mediated inhibition.

Methods

In RESULTS, we analyze the effect of inhibition on burst firing using phase plane methods. Strictly speaking, phase plane methods are only appropriate for use on two-dimensional equation systems. We may apply these methods to the pyramidal cell model, however, by restricting the analysis to the silent phase of bursting. During the silent phase, several variables are approximately constant so that each compartment reduces to essentially a two-dimensional system. Specifically, in the soma compartment during the silent phase, the sodium inactivation variable h is approximately 1 and does not change significantly until somatic voltage increases past 0 mV, near the peak of the leading sodium spike of the burst. Thus, leading up to burst initiation, the soma dynamics are governed by the V_s and n equations. Similarly, the dendrite dynamics during the silent phase are essentially governed by the V_d and q equations. The gating variables s and c of the calcium current and the voltage-activated potassium current, respectively, are approximately 0, as is Ca^{2+} concentration Ca. By restricting our attention to the silent phase of bursting, leading up to burst initiation, we may consider the soma trajectory in the $V_s - n$ phase plane and the dendrite trajectory in the $V_d - q$ phase plane.

In phase plane analysis of single compartment models, the trajectory is governed by the position of the nullclines of each equation, and these nullclines are stationary for fixed values of parameters. For our phase plane analysis of this two-compartment model, we consider separate phase planes for each compartment, and the trajectory for each compartment is determined by the position of its respective nullclines. But the compartments, and thus their phase planes, are linked through the coupling current, $I_{\text{coup}} = g_c(V_d - V_s)/p$. As the voltages evolve, the coupling current continuously changes. Hence the nullclines in each phase plane are not stationary but are continuously moving. During the silent phase, both voltages, and thus I_{coup}, evolve slowly, and we can track trajectories in each phase plane relative to slowly moving nullclines.

Another difference in the phase plane analysis of a two-compartment model compared to that of a single compartment model is the effect of brief synaptic current. In a single compartment model, inhibitory synaptic current, for example, shifts down the voltage equation nullcline, which generally has a cubic shape. When the synaptic current shuts off, the cubic nullcline returns to its original position. In the two-compartment model, inhibitory synaptic input to one of the compartments has a similar effect of shifting the cubic nullcline down. But when the synaptic current shuts off, the nullcline may not return to its original position because the voltages in each compartment, and thus I_{coup}, are not the same as before the synaptic input.

RESULTS

Inhibition arriving before a burst delays burst firing

We consider the effect of a single dose of synaptic inhibition arriving during the interburst interval on the timing of subsequent burst firing. We consider the pyramidal cell-interneuron network structure with one synaptic connection from the interneuron to the dendrite compartment ($g_{\text{inh}} = 1$ and $g_{\text{exc}} = 0$ mS/cm^2). The interneuron is made to fire by giving it a brief applied current pulse of sufficient magnitude to generate a single action potential. The soma voltage traces in Fig. 2, *A–C*, show a delay in burst firing caused by the inhibition. In Fig. 2*A*, no inhibition is given, and the pyramidal cell displays very low-frequency, periodic bursting. In Fig. 2, *B* and *C*, the interneuron is stimulated so that inhibition arrives before py-

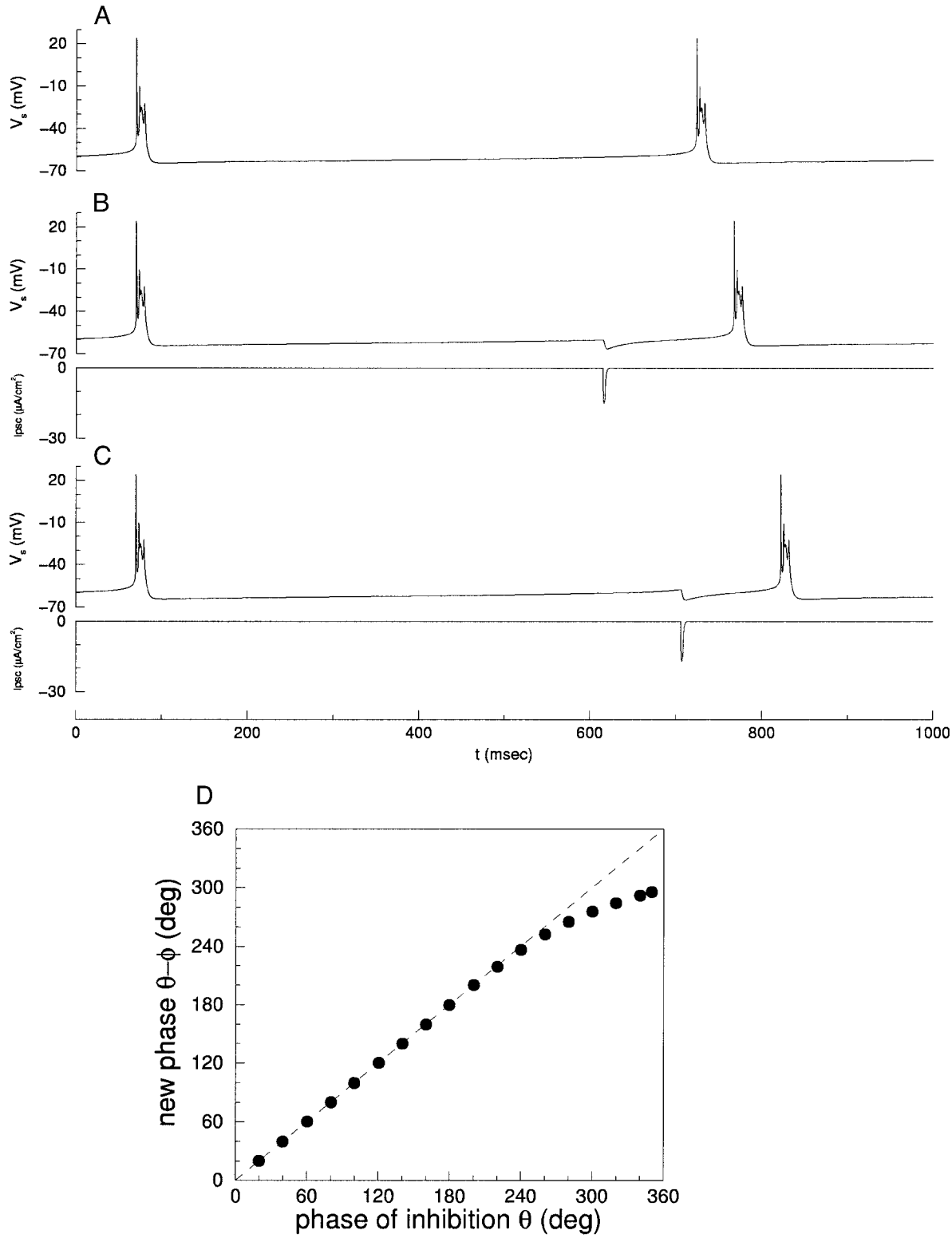

FIG. 2. Delay in timing of burst firing due to synaptic inhibition given before burst firing (g_{inh} = 1 and g_{exc} = 0 mS/cm^2). *A*: pyramidal cell bursting at very low frequency with no inhibition given (soma voltage shown). *B* and *C*: interneuron fires at phases θ = 300° (*B*) and 350° (*C*), causing phase delays of approximately 24° (*B*) and 55° (*C*) in somatic burst firing [*top trace*: soma voltage; *bottom trace*: inhibitory postsynaptic current (IPSC) received at the dendrite compartment]. *D*: phase resetting curve plotting new phase $\theta - \phi$ in response to inhibition arriving at different phases θ in the burst cycle, where ϕ is phase delay.

ramidal cell firing. The *bottom traces* show the inhibitory postsynaptic current (IPSC) at the dendrite compartment. Since the synapse is fast and no synaptic delay is modeled, there is only a 1- to 2-ms lag between the applied current pulse to the interneuron and the IPSC in the dendrite compartment. Also note that the inhibition decays quickly. The synaptic inhibition

delays firing of the next burst with the amount of delay depending on its time of arrival. Figure 2*D* shows a summary of this effect as a phase resetting curve where the phase that inhibition arrives θ is plotted on the *x*-axis, and the resultant new phase after inhibition is plotted on the *y*-axis. To interpret the diagram, we associate 360° in phase to the intrinsic period of the pyramidal cell. We calculate the time difference between when the inhibited pyramidal cell fires and when it would have fired in the absence of inhibition. This time is then converted to a phase ϕ. The new phase is $\theta - \phi$. If inhibition arrives immediately following a burst and up to approximately 260° in the burst cycle, it has virtually no effect on burst firing as seen by the new phase being approximately equal to the old phase. When inhibition arrives closer to the time of burst firing, it delays the next burst, thus shifting its phase back. The amount of delay or phase shift increases as the timing of inhibition approaches the time of burst firing with a maximal delay, with this set of model parameters, of about 55° or 100 ms.

A similar delay effect of inhibition is obtained when the intrinsic frequency of the pyramidal cell is varied by changing the value of the applied current to the soma compartment I_s. For I_s values between approximately -0.2 and 1.3 μA/cm^2, where the pyramidal cell displays very low-frequency bursting in the range from 0.4 to 4 Hz, inhibition arriving during the interburst interval delays the following burst, and the amount of delay increases as the timing of inhibition approaches the time of firing. The maximal delay obtained and the range of phases where the delay is observed depends on the intrinsic burst frequency. For example, for higher intrinsic frequencies obtained with larger values of I_s, delays are first observed at earlier phases, and the maximal phase delay is larger.

In this study, we consider the inhibition arriving to the dendrite compartment. The same delay effect is obtained if the inhibition arrives instead to the soma compartment. In fact, the phase where delays are first observed and the maximal phase delay are basically the same as those obtained above.

An interesting result of this effect is that if the inhibition is periodic such that it always arrives at the same phase of the burst cycle, pyramidal cell firing can be entrained to a lower frequency. For example, if the interneuron is paced to fire with a slightly longer period than the intrinsic pyramidal cell burst period and the interneuron fires at a phase between 260° up to 360° of the burst cycle such that the phase delay is equivalent to the difference in periods, then the pyramidal cell will always be inhibited at the same phase, and firing will be entrained to the lower interneuron frequency. We have previously proved that fast synaptic inhibition can entrain a simple neuron model to a lower frequency than its intrinsic firing frequency and that the lower frequency firing is a stable periodic orbit (Bose et al. 2000). A similar proof may be applied to the present network model to show that the lower frequency firing is a stable state. With these values of model parameters, periodic synaptic inhibition arriving once during the interburst interval can entrain the pyramidal cell to fire at frequencies in the range from almost 1.3 to 1.5 Hz, where the intrinsic burst frequency is approximately 1.5 Hz (simulations not shown). We note that if the inhibition arrives at a sufficiently high frequency, the pyramidal cell frequency can be made arbitrarily small or even completely suppressed.

In the following paragraphs, we analyze how synaptic inhibition causes the delay in firing in the two-compartment pyramidal cell model with phase plane methods, starting with an analysis of burst initiation. An interesting insight revealed by this analysis is a subtle difference in the mechanism of burst initiation than is described in the original model paper (Pinsky and Rinzel 1994). In the very low-frequency bursting regime, Pinsky and Rinzel (1994) describe that the duration of the silent phase is determined by the potassium AHP current in the dendrite compartment. In particular, they propose that when the slow gating variable, q, for this current passes below a threshold value, a somatic sodium spike is triggered, thus initiating a burst. Our analysis shows that while the decay of the gating variable q governs the duration of the silent phase, it is actually the resulting slow rise in V_d that leads to burst initiation. So, instead of there being a threshold value for q, there is a V_d threshold, V_d^*, that must be crossed to trigger the leading sodium spike of the burst. In a normal burst cycle, the slow rise in V_d is determined primarily by the decrease in q, but inhibition arriving before a burst decouples V_d from q, thus revealing this distinction.

For our phase plane analysis, we refer to the soma compartment $V_s - n$ and dendrite compartment $V_d - q$ phase planes shown in Fig. 3. In both phase planes, the burst trajectory of Fig. 2*C* is shown by the heavy curve (arrows indicate flow direction). At the beginning of the silent phase (indicated by "sp" in Fig. 3, *A* and *B*), V_s and V_d are hyperpolarized resulting in a hyperpolarizing coupling current in each compartment that pushes the V_s and V_d cubic nullclines down to the positions at the lower boundaries of the shaded regions. In the soma compartment $V_s - n$ phase plane, the local minima or left knee of the V_s cubic is below the *n*-nullcline (thin dashed curve). This results in a fixed point on the lefthand branch of the V_s cubic at the intersection of the two nullclines, which prohibits the soma from spiking. Because of the fast dynamics in the soma compartment, the soma trajectory moves to within a small neighborhood of this fixed point at the beginning of the silent phase.

During the silent phase, the electrotonic coupling between compartments causes a slow evolution of the cubic nullclines in each phase plane. As V_s and V_d depolarize during the silent phase (solid portion of trajectory curves), the coupling current increases and the cubic nullclines slowly move up through the shaded regions (direction indicated by long arrows). The dendrite trajectory moves down the lefthand branch of the slowly rising V_d cubic and the soma trajectory tracks the fixed point at the intersection of the slowly rising V_s cubic and the *n*-nullcline. Note that the trajectory in the $V_d - q$ plane remains away from the knees of the V_d cubic nullcline (Fig. 3*C*) as is expected since firing is initiated in the soma compartment.

Let $I_{\text{coup}} = g_c(V_d - V_s)/p$ denote the coupling current in the soma compartment. For the uninhibited trajectory, I_{coup} reaches a critical value I_{coup}^* when the left knee of the V_s cubic becomes tangent to the *n*-nullcline. The position of the cubic nullclines at this point is indicated by the upper boundaries of the shaded regions in Fig. 3. Let V_s^* be the value of V_s at the point of tangency of the V_s and n nullclines, also called a saddle-node point. When I_{coup} increases through I_{coup}^*, the fixed point on the V_s nullcline disappears and, provided that V_s is near V_s^*, the soma can trigger the leading spike of the burst. In the uninhibited trajectory, since the soma voltage is at V_s^* when $I_{\text{coup}} = I_{\text{coup}}^*$, this defines a threshold value for dendrite voltage at burst initiation, V_d^*.

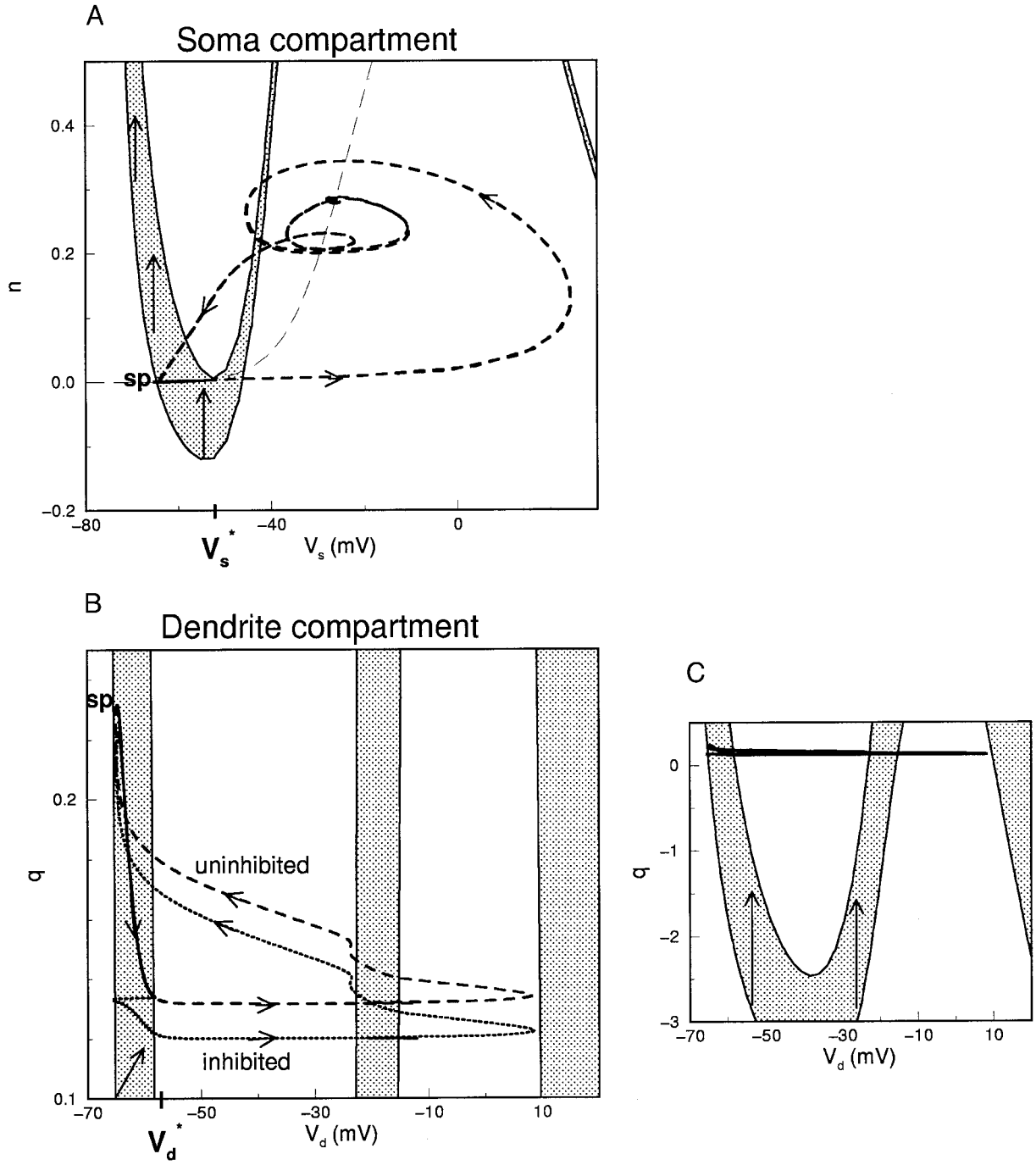

FIG. 3. Phase plane analysis of silent phase of complex burst cycle. In *A* and *B*, solid bold portion of curve indicates silent phase where phase plane analysis is valid. In *A–C*, during silent phase V_s and V_d cubic nullclines slowly rise through shaded regions due to coupling current between compartments (long arrows indicate direction). Nullclines at lower boundaries of shaded regions indicate position at beginning of silent phase (labeled by "sp" on trajectory) and curves at upper boundaries indicate positions at burst initiation. *A*: soma voltage trajectory of Fig. 2*C* (heavy curve, short arrows indicate flow direction) projected in $V_s - n$ phase plane. *n* nullcline shown by dashed curve. A somatic sodium spike is triggered after the fixed point at the intersection of the cubic nullcline, and the *n* nullcline disappears at V_s^*. *B*: dendritic voltage trajectory of Fig. 2*C* projected into the $V_d - q$ phase plane. Inhibition is given just prior to burst firing. The top trajectory (dashed curve) indicates the uninhibited burst trajectory. The bottom trajectory (dotted curve) is the burst trajectory delayed by inhibition. Both voltages evolve along the same trajectory in the silent phase until the moment the delayed trajectory feels inhibition causing its V_d value to hyperpolarize. For both cases, the complex burst is initiated when $V_d = V_d^*$. *C*: a zoom out of *B*. Burst initiation occurs when trajectory is far away from the left knee of the V_d cubic.

We can summarize by stating two conditions for burst initiation: *1*) V_s must be sufficiently close to V_s^* and *2*) I_{coup} must be greater than I_{coup}^*. Since *condition 1* is satisfied in the silent phase, *condition 2* reduces to $V_d > V_d^*$. Pinsky and Rinzel's description of burst initiation caused by q decreasing below a threshold value is consistent with these two conditions. In the intrinsic burst trajectory, since decreasing q governs the rise in V_d, an equivalent q threshold can be defined as the q value on

the upper boundary of the shaded region in Fig. 3*B* at $V_d = V_d^*$. However, for the case of synaptic inhibition given before the burst, we will show that a true threshold in q does not exist.

The cause of delay in burst firing when inhibition is given during the silent phase before a burst can now be described (Fig. 3*B*, dotted curve shows inhibited trajectory). In response to inhibition, the V_d cubic nullcline is quickly shifted down. Depending on the strength of inhibition, the cubic may be shifted to a position below or within the shaded region (not explicitly shown in the figure). The V_d trajectory approximately follows the shifted nullcline (note the sharp V_d decrease in $V_d - q$ trajectory in Fig. 3*B*). This decrease in V_d, and hence I_{coup}, shifts the V_s cubic down to a position below or within the shaded region (not explicitly shown). The soma trajectory continues to track the fixed point as it is moved to lower V_s (since the trajectory moves back along the same path that it had been traveling, this shift in V_s is not apparent in the figure). The slow variable q is not dependent on V_d and thus continues to decrease. When the inhibition shuts off, the V_d nullcline will quickly rise. It does not return to its position before the synaptic event, however, because now V_s, V_d, and hence the coupling current are at different values than before the inhibition. The overall effect of the inhibition is to shift both the V_d and V_s cubic nullclines down, forcing the trajectories to evolve along the cubic nullclines as they slowly move up through the shaded region. Since the soma trajectory remains close to the fixed point on the V_s cubic, *condition 1* for burst firing is still satisfied after the inhibition. The delay in firing is caused by the additional time needed for *condition 2* to be satisfied, namely for V_d to increase past V_d^*. During this time, q continues to decrease, passing below the nominal threshold value determined by the intrinsic trajectory. Thus it is clear that it is more appropriate to think about a threshold value for V_d for burst initiation rather than a threshold value for q.

We note that due to this delay effect of inhibition, this model cell is not able to fire via postinhibitory rebound in the strict sense. Namely, the cell does not immediately fire when it is released from inhibition, regardless of when the inhibition is given.

Inhibition arriving during burst causes advance in burst firing and modulates burst waveform

We now consider the effect of inhibition arriving during a burst, specifically arriving just following the leading spike of the burst. We achieve this timing for the inhibition with the network structure in which there is an excitatory synaptic connection from the soma compartment of the pyramidal cell to the interneuron (g_{exc} nonzero) and an inhibitory synaptic connection from the interneuron back to the dendrite compartment (g_{inh} nonzero). In this network, pyramidal cell firing causes the interneuron to spike, thus sending inhibitory synaptic current back to the dendrite compartment of the pyramidal cell (Fig. 1). Since there is no synaptic delay modeled, the inhibition arrives just after the leading spike of the burst.

As shown in Fig. 4, *A* and *B*, such feedback inhibition during a burst causes an advance in the firing of the subsequent burst. When the pyramidal cell is repetitively bursting, as it is in Fig. 4 (uninhibited firing shown in *A*), the feedback inhibition advances each burst and higher frequency repetitive bursting can be obtained (Fig. 4*B*, *top trace*). The brief IPSC in the dendrite compartment as a result of interneuron firing is shown in the *bottom trace* of Fig. 4*B*. The amount of phase advance depends on the strength of inhibition that is controlled by g_{inh}. As g_{inh} increases from zero to 0.45 mS/cm^2, the phase advance increases to, in this case, approximately 120°, equivalent to decreasing the period by 215 ms. This phase advance by inhibition is summarized in the phase response plot shown in Fig. 5*A*. In this figure, the new phase resulting from the inhibition is plotted versus strength of inhibition, g_{inh}. The data points marked with "C" (for complex burst) show the increase in phase advance of bursting as g_{inh} is increased from 0 to 0.45 mS/cm^2. Another way to view these results is in the plot of steady-state burst frequency shown in Fig. 5*B*. In this plot, the "C" data points show the increase in burst frequency from approximately 1.5 to 2.3 Hz as g_{inh} is increased from 0 to 0.45 mS/cm^2.

When g_{inh} is increased past 0.45 mS/cm^2, the phase advance continues to increase, and, furthermore, the burst waveform is modified. We find a smooth transition from a full complex burst ($0 \leq g_{\text{inh}} \leq 0.45$, Fig. 4, *A* and *B*) to bursts consisting of 4 spikes ($g_{\text{inh}} = 0.5$, Fig. 4*C*) and 3 spikes ($g_{\text{inh}} = 0.51$, *D*), to bursts with 2 spikes or spike doublets ($g_{\text{inh}} = 0.53$, *E*), to single spikes ($g_{\text{inh}} \geq 0.57$, *F*). Occurring with these changes in burst profile is an increase in phase advance of the subsequent burst, from approximately 120° for the complex burst when $g_{\text{inh}} = 0.45$ to 310° for the single spike when $g_{\text{inh}} = 1$ mS/cm^2. When the pyramidal cell is repetitively bursting, as it is here, these phase advances correspond to an increase in burst frequency from 2.3 Hz when $g_{\text{inh}} = 0.45$ to over 11 Hz when $g_{\text{inh}} = 1$ mS/cm^2. We again refer to Fig. 5, *A* and *B*, to summarize the increases in phase advance and frequency, respectively, with increasing g_{inh}. In the figures, the number at each data point indicates the number of spikes per burst. Combining these results with those from the previous section, inhibition can entrain the pyramidal cell to fire in a range from arbitrarily low frequencies up to 11 Hz.

We obtain similar phase advances and modulation of waveform for different intrinsic burst frequencies of the pyramidal cell when the applied current to the soma I_s is changed. But the values of g_{inh} where the effects occur are different. For example, when the intrinsic burst frequency of the pyramidal cell is higher ($I_s = 0.75$ μA/cm^2), the transitions in waveform occur at lower values of g_{inh}, and the phase advances occurring with the waveform changes are larger. The transitions in waveform, however, are not smooth. As g_{inh} is increased, complex bursting gives way to irregular firing of 3 spike bursts and doublets. Periodic firing of bursts with 4 or 3 spikes are not observed in this case. But as g_{inh} is increased further, periodic firing of spike doublets and single spikes is obtained. In general, for all values of I_s, regular spike doublet and single spike firing is obtained for high values of g_{inh}.

We also obtain similar phase advances and similar modulation of waveform as inhibition is strengthened when the inhibition arrives at the soma compartment instead of at the dendrite. Again, the values of g_{inh} where similar results are observed are different, but phase advances and regular firing of the same types of burst waveforms are obtained. For example, in the case shown here, if inhibition arrives to the soma compartment, the transition from complex bursting to regular firing of bursts with 4 spikes occurs at a higher g_{inh} value, and the range of g_{inh} values over which 4-spike bursts are obtained

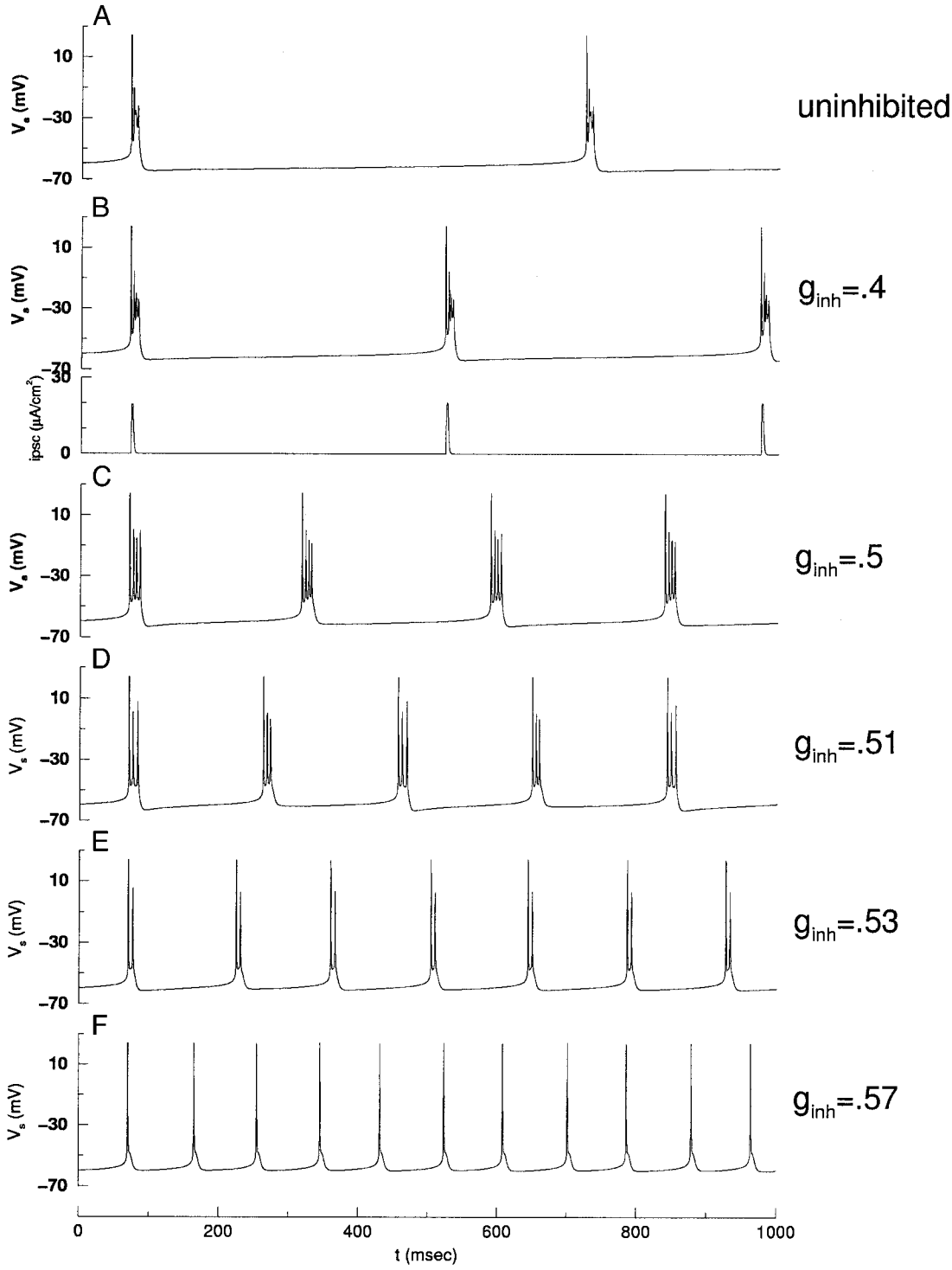

FIG. 4. Advance in timing of burst firing and modulation of burst waveform due to synaptic inhibition given during burst. *A–F*: soma voltages shown, g_{exc} = 5 mS/cm^2, g_{inh} values given in mS/cm^2. *A*: with no inhibition given, pyramidal cell fires complex bursts at very low frequency. *B*: weak inhibition (g_{inh} = 0.4) arriving during bursts (IPSC received at dendrite compartment shown in *bottom trace*) phase advances following bursts by approximately 110°. *C–F*: with stronger inhibition during burst (IPSCs are similar to *B* but with slightly larger amplitudes), burst waveform is modulated and phase advance increases as follows: (*C*, g_{inh} = 0.5) 4-spike bursts with phase advances of 220°, (*D*, g_{inh} = 0.51) 3-spike bursts with 253° advances, (*E*, g_{inh} = 0.53) spike doublets with 282° advances, and (*F*, g_{inh} = 0.57) single spikes with 310° advances.

is larger. As g_{inh} is increased further, regular firing of 3-spike bursts and spike doublets are obtained over larger ranges of g_{inh} values.

To understand the phase advance caused by inhibition, we recall that in this model a burst is generated by dendritic, calcium-based depolarization supporting somatic, sodium spiking. The general effect of inhibition arriving just after burst initiation is to lessen dendritic depolarization. This attenuation

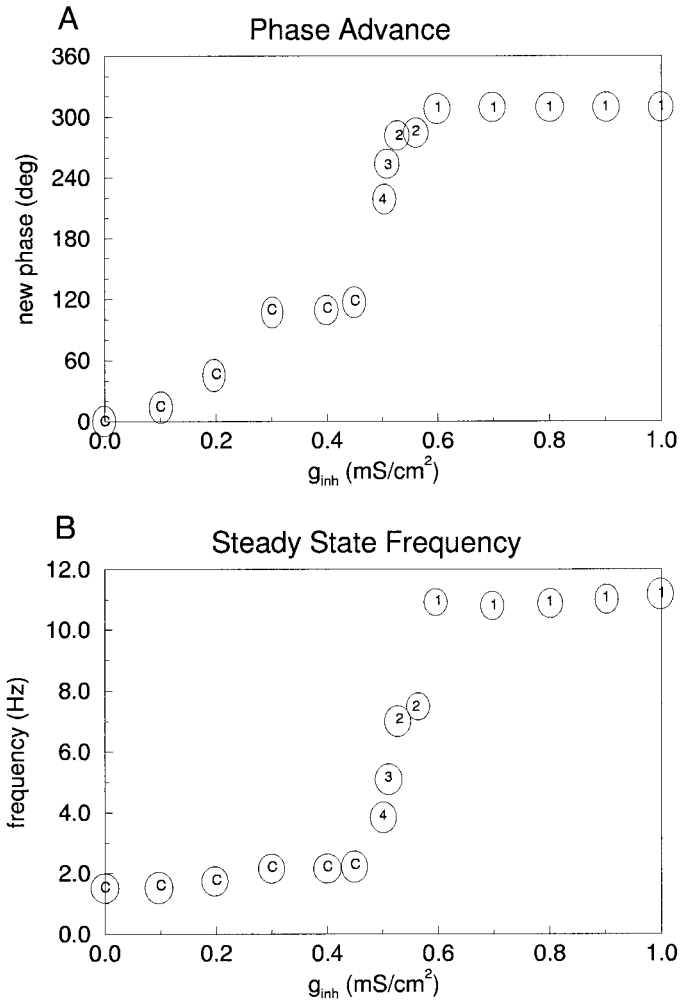

FIG. 5. Phase advances caused by inhibition given during burst (*A*) and resultant steady-state frequency of burst firing (*B*) as strength of inhibition (g_{inh}) is varied. Data points marked with 'c' indicate full complex bursts. Numbers at other g_{inh} value indicate number of spikes per burst as burst waveform is modulated.

of peak V_d when $g_{inh} = 0.4$ mS/cm^2 compared to the uninhibited case can be seen when both trajectories are plotted in the dendrite compartment $V_d - q$ phase plane (Fig. 6*A*) and in a time plot (Fig. 6*G*, bursts are offset for comparison purposes). We note that strict phase plane analysis of solutions is only appropriate during the silent phase of bursting, but we find that plotting the trajectories in their phase planes is helpful in understanding effects of inhibition during the burst. As a result of the inhibition, Ca^{2+} influx is suppressed during the burst (Fig. 6*B*), which causes less activation of the slow potassium AHP current with gating variable q (Fig. 6*C*). The inhibition acts during the active phase of the burst (Fig. 6*G*, heavy bars under bursts indicate duration of IPSC) and has decayed away by the time the cell returns to the silent phase. Thus, in the silent phase (Fig. 6*A*, beginning indicated by "sp"), the cell will track the nullclines corresponding to the intrinsic burst case in the $V_d - q$ phase plane (heavy portion of dotted curve). As discussed in the previous section, when no inhibition is given, the control of the rise of V_d by q during the silent phase determines the duration of the interburst interval. The inhibition induced attenuation of the *Ca* and q peaks shortens the subsequent silent phase of the burst cycle since, as can be seen in the $V_d - q$ phase plane, the inhibited trajectory begins the silent phase (heavy portion of solid curve) at a lower value of q and higher value of V_d. Thus it takes less time for V_d to cross V_d^* and trigger a somatic spike.

The change in burst profile with increasing g_{inh} occurs similarly by an attenuation of dendritic depolarization. When g_{inh} is small ($g_{inh} = 0.4$ mS/cm^2, for example), the inhibition is not strong enough to prevent a V_d Ca^{2+}-based spike. So while peak V_d is attenuated compared to the uninhibited case, it is still large enough to overdrive the soma spike generator and create a complex burst (Fig. 6*G*, 1st 2 bursts). If, however, g_{inh} is large ($g_{inh} \geq 0.57$, for example), the inhibition abolishes the V_d Ca^{2+}-based spike, and only the leading sodium spike of the burst is realized. As can be seen in the $V_d - q$ phase plane (Fig. 6*D*, solid curve) and in a time plot (Fig. 6*G*, last burst), there is a V_d spike due to backpropagation of the leading sodium spike, but the dendritic response has been inhibited. The leading spike allows a minimal *Ca* increase (Fig. 6*E*, solid curve) and thus a small increase in q (Fig. 6*F*, solid curve).

For intermediate values of g_{inh} ($0.5 \leq g_{inh} \leq 0.56$ mS/cm^2), the dynamics are more interesting. In these cases, the inhibition is strong enough to prevent the initiation of a full V_d Ca^{2+}-based spike, but is not strong enough to completely hyperpolarize the dendrite. The partial depolarization of the dendrite allows soma-dendritic ping-pong interactions to support a burst. For example, when $g_{inh} = 0.51$ mS/cm^2, the leading V_d spike, shown in the $V_d - q$ phase plane (Fig. 6*D*, dashed curve) and in a time plot (Fig. 6*G*, 4th burst), is the same as for larger g_{inh}, but the weaker inhibition allows the dendrite to remain sufficiently depolarized to support another sodium spike. The backpropagation of this second sodium spike again sufficiently depolarizes the dendrite providing for a third sodium spike. This ping-pong effect does not continue indefinitely since dendritic depolarization and calcium influx (Fig. 6*E*, dashed curve) trigger the I_{K-C} current, which ultimately ends the burst. Similar dynamics account for the 4-spike bursts (Fig. 6*G*, 3rd burst) and spike doublets that are observed for g_{inh} values in this intermediate range.

Pinsky and Rinzel (1994) showed that by increasing applied current to the soma I_s, to mimic *N*-methyl-D-aspartate (NMDA) excitation, the pyramidal cell changes from a bursting mode to a single spiking mode with frequencies between 20 and 30 Hz. The changes effected by increasing I_s resulted from an essential shutdown of the dendritic calcium-based mechanisms. At high values of I_s, the dendrite and soma spike at the same frequency, causing low-amplitude, fast oscillations in calcium concentration. These changes in *Ca* are sufficiently fast such that the slow gating variable q of the AHP current remains at a constant level. Even though the constant q level is relatively high, near peak values in the bursting mode, the AHP current does not participate in the afterhyperpolarization of spikes or affect the interspike interval. Also, any hyperpolarizing effect on the soma compartment by the AHP current is counteracted by the high somatic applied current. To summarize their results, tonic somatic depolarization weakens the effect of the dendritic compartment. In our model, fast synaptic inhibition to the dendrite provides a similar regulation of dendritic calcium mechanisms. However, the frequency of single spikes that we obtain is significantly lower than what Pinsky and Rinzel (1994) obtain with large I_s. The reason is that even though calcium concentration remains at low levels, the AHP gating

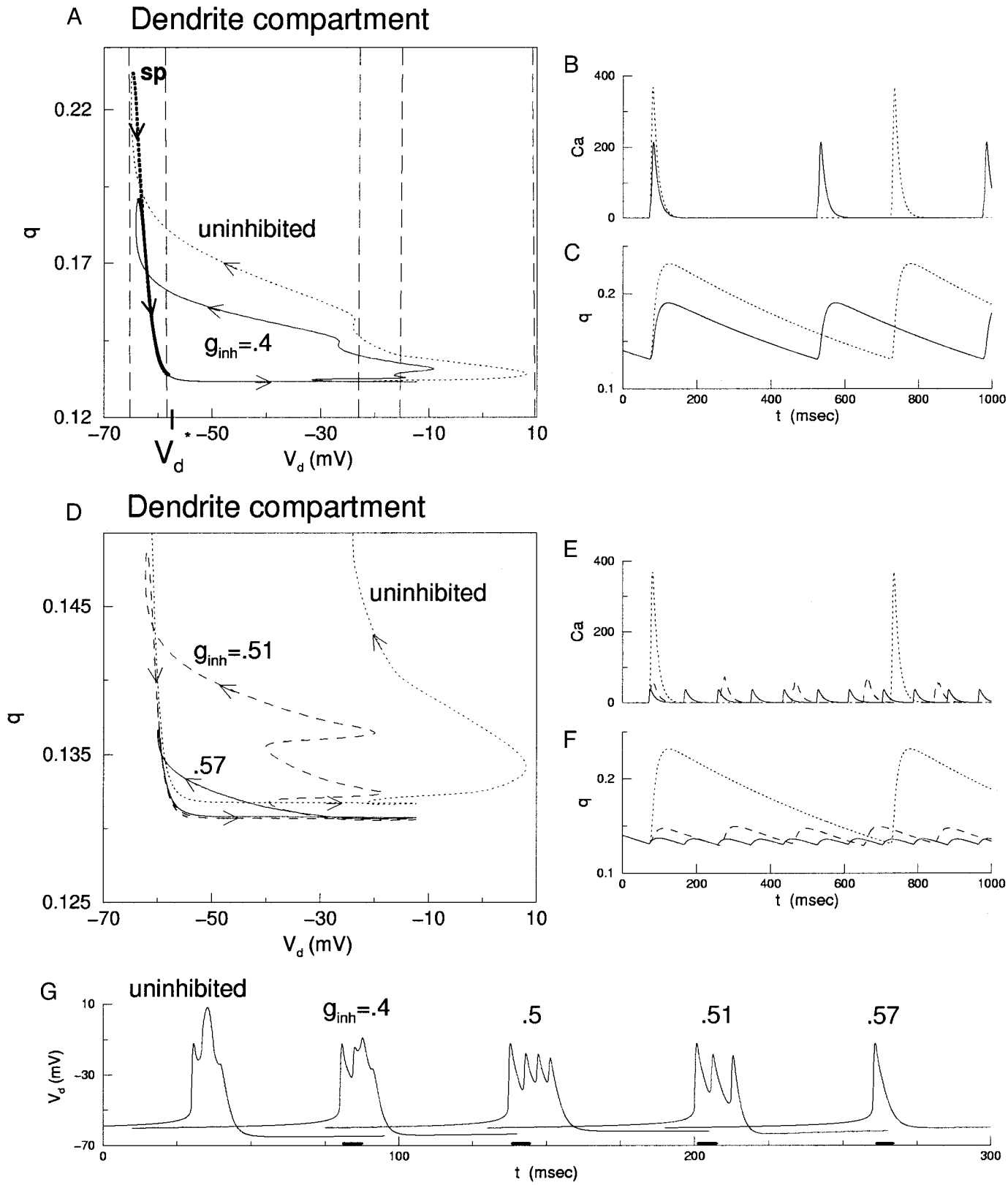

FIG. 6. Burst trajectories with inhibition arriving during the burst plotted in dendrite compartment $V_d - q$ phase plane. *A* and *D*: trajectories from simulations in Fig. 4 shown in $V_d - q$ plane. *A*: Figs. 4*A* (· · ·) and 4*B* (———), bold portion of trajectories indicates silent phase (beginning labeled by "sp"), cubic V_d nullclines and location of V_d^* shown for reference. *D*: Figs. 4*A* (· · ·), 4*D* (– – –), and 4*F* (———); g_{inh} values given in mS/cm^2. *B*, *C*, *E*, and *F*: corresponding time traces of dendritic intracellular Ca^{2+} concentration, *Ca* (*B* and *E*) and of dendritic potassium afterhyperpolarization current gating variable, *q* (*C* and *F*). *G*: dendritic voltage traces from simulations in Fig. 4, *A–D* and *F*, showing the effect of inhibition. Traces are offset for comparison purposes. Heavy bar under bursts indicates duration of IPSC in dendrite compartment.

variable q is activated with every spike and participates in spike afterhyperpolarization and determination of the interspike interval since somatic applied current levels are low.

Synchronous and out-of-phase oscillations in networks of pyramidal cells

Pinsky and Rinzel (1994) show that a network consisting of a number of their two-compartment pyramidal cells can exhibit synchronous or near-synchronous oscillations if the pyramidal cells have recurrent AMPA-mediated excitatory connections. This mechanism for synchrony was also previously observed by Traub et al. (1991) in their large-scale computational model. By blocking AMPA in those studies, the cells desynchronize. These studies did not include the effect of inhibition in promoting relevant rhythmic patterns. We show here that there is an alternate mechanism that may promote synchrony among the pyramidal cells; namely slowly decaying inhibitory input can be used to synchronize pyramidal cells that are weakly connected or even unconnected.

We consider two pyramidal cells that each have reciprocal synapses onto the same interneuron (Fig. 7*A*). The interneuron makes an inhibitory synaptic connection to the dendrite compartment of each pyramidal cell and an excitatory synaptic current is sent from the soma compartments of each pyramidal cell back to the interneuron. The pyramidal cells initially are assumed to have no excitatory connections between themselves. We focus on two specific rhythm patterns; synchronous and out-of-phase oscillations.

Figure 7*B* shows the voltage traces of the two pyramidal cells P_1 and P_2. The simulation shows that the cells start out-of-phase with one another, but that their burst envelopes quickly synchronize after the first few cycles. Both cells receive a common slowly decaying inhibition from the interneuron I (decay rate of synaptic gating decreased to $\beta = 0.1$ mS^{-1}). Slowly decaying inhibition is known to synchronize cells when both cells receive the inhibition from a common inhibitory cell, but in situations where neither cell synapses back to the inhibitory cell (Terman et al. 1996). If the cells do synapse on the interneuron, for one-compartment models, a delay to the onset of inhibition is necessary for synchrony (Rubin and Terman 2000; Terman et al. 1998; van Vreeswijk et al. 1994). In our model, we do not require an explicit delay, because the separation of the soma and dendrite provides an "effective delay" to the onset of inhibition. In particular, the inhibition acts to hyperpolarize the dendrites, which then hyperpolarizes the soma via the coupling current. The speed with which the inhibition ultimately affects the soma is dependent on the intrinsic properties of the dendrite (the rate at which it hyperpolarizes) and the strength of the electrical coupling. If either of these quantities is small, then there effectively will be a small window of time from when the inhibitory cell fired to the time the soma receives the full impact of this input. During this time, the soma will be able to fire a sodium spike, thus initiating the burst. This delay plays the same role that explicit synaptic delays play in Terman et al. (1998) and Rubin and Terman (2000). The slowly decaying inhibition has the effect of keeping the dendritic voltages of each cell close to one another. As we showed earlier, the dendrite voltage must cross V_d^* in order for the soma to fire. The slowly decaying inhibition allows the dendritic voltages of each cell to compress and cross this threshold within a small time window of one another. By varying the maximal conductance of the inhibitory synapse, we also obtain synchrony between the cells during complex burst mode, single spike mode, and multiple spike mode (simulations not shown). We note that to achieve synchrony in the burst mode, a much slower decay of inhibition is necessary relative to the decay rate for synchrony of single spikes. In the burst mode, the dendrite voltage trajectories return to the silent

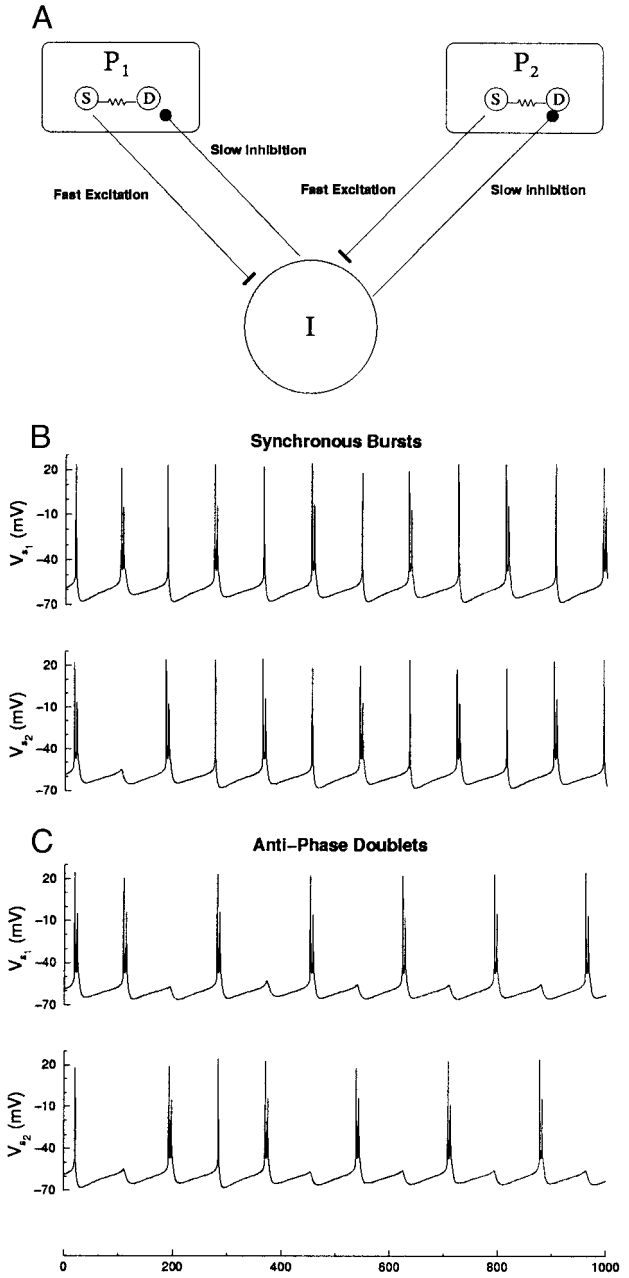

FIG. 7. *A*: the 3-cell network. The soma compartments of both pyramidal cells make fast excitatory synapses onto a common inhibitory interneuron. The interneuron makes a fast inhibitory synapse onto the dendrite compartment of each pyramidal cell. *B*: synchronous oscillations. Traces show the somatic voltages of each of the pyramidal cells. The burst envelopes of the cells become and then remain synchronized throughout the simulation, but the number of spikes within each burst alternates from cycle to cycle. *C*: anti-phase oscillations. Traces show the same cells, with the same parameter values, but different initial conditions than *B*, firing anti-phase doublets. For *B* and *C*, $I_s = 0.5$, $\beta = 0.1$, $g_{inh} = 0.5$ mS/cm^2, and $g_{exc} = 5.0$ mS/cm^2.

phase with low V_d and high q values. If the inhibition decays quickly, the dendrite trajectories will quickly follow that of an uninhibited dendrite, as depicted in Fig. 2*B*. In this case, there will be no compression between V_d trajectories. Alternatively, this type of inhibition can synchronize single spiking cells since they return to the silent state with higher V_d and lower q values. Thus the quickly decaying inhibition will now act to delay the next spikes, as in Fig. 2*B*, which allows compression of the V_d trajectories to occur.

Figure 7*C* shows the two cells oscillating in anti-phase with one another. The parameter values are the same as those for the synchronous oscillations. Thus the network exhibits bistability of periodic solutions. The bistability is produced much in the same way as for one-compartment relaxation oscillator models. The synchronous solution arises as discussed above if the dendritic voltages start out sufficiently close together. If these voltages are not close, then an anti-phase, and, more generally, an out-of-phase solution arises. In this case, the firing of P_1, for example, causes P_2 to receive an inhibitory input before it were to fire. This, as depicted in Fig. 2*B*, may cause a delay of the P_2 burst. Thus during the time P_1 is active, P_2 is moved away from its firing threshold. Similarly when P_2 fires, it delays the onset of a P_1 burst. Moreover, depending on the strength of the inhibition, the firing pattern of each cell within its burst is also modulated as described previously.

The addition of weak excitatory coupling between the pyramidal cells does not change the qualitative behavior described above. However, it can change the firing pattern within a burst of each cell. Weak excitation lessens the overall level of hyperpolarization due to the interneuron, if both excitation and inhibition wear off on similar time scales. As seen above, the firing pattern of the cells is sensitive to small changes in the maximal conductance of the inhibitory synapse. As a result, weakly connected pyramidal cells that may have fired spike doublets while unconnected, may now fire bursts with more spikes due to the changed balance between excitation and inhibition (simulations not shown).

DISCUSSION

We have shown that, depending on its timing, synaptic inhibition may delay or advance burst firing in a model pyramidal cell. As a result, periodically timed inhibition can either increase or decrease the firing frequency of a repetitively bursting neuron within a range around the intrinsic bursting frequency. Increasing burst frequency requires inhibition to arrive at the beginning of a burst, following the initial sodium spike. In this case, we generate periodic inhibition as a result of the reciprocal synaptic connections between the pyramidal cell and the interneuron. Thus the source of periodic inhibition is the repetitive firing of the pyramidal cell itself. Decreasing burst frequency, on the other hand, requires that inhibition arrive before burst firing, at a constant phase of the burst cycle. This can be achieved if the interneuron fires periodically at a lower frequency than the intrinsic frequency of the pyramidal cell. A possible source for periodic inhibition in this case may be the theta rhythm. It is known that cells in the medial septum make GABAergic connections to interneurons in CA3 and act as a pacemaker drive for the theta rhythm (Green and Arduini 1954). If the intrinsic frequency of the pyramidal cell is greater than theta frequency, interneurons driven to fire at theta frequencies could provide the appropriate periodic inhibition to decrease pyramidal cell frequency.

Our results show that slowly decaying inhibition can be used to synchronize the activity of pairs of pyramidal cells. The results suggest an alternative to the explanation of Pinsky and Rinzel (1994) and Traub et al. (1991) that fast excitatory AMPA-mediated synapses between these cells are responsible for synchrony. The synchronization of actual CA3 cells could be reflective of a two-step process; the first is recruitment of co-active place cells due to excitatory synapses; the second is maintenance of the synchrony due to slowly decaying inhibition. Synchrony ranges from complex bursts to single spikes, thus encompassing the full range of firing behaviors detailed in Fig. 4. Moreover, there is no difficulty in generalizing the synchrony result to larger networks of pyramidal cells.

An experiment that would investigate whether inhibitory interneurons participate in synchronizing pyramidal cells in CA3 would be to stimulate a single interneuron and record from two or more of its target pyramidal cells. It has been shown in CA1, that a single interneuron can entrain the firing of two target pyramidal cells in vitro (Cobb et al. 1995). Similarly, in CA3, we may expect that if AMPA and NMDA receptors are blocked, we would observe synchronous inhibitory postsynaptic potentials (IPSPs) in the target pyramidal cells entraining their firing. Additional experiments where certain synaptic receptors are blocked and then washed out could further indicate the contributions of both inhibitory and excitatory inputs to network synchrony.

The delay/advance of bursts due to inhibitory input can also be achieved in simpler mathematical models, such as relaxation oscillators. With these models, inhibition applied during a burst tends to shorten the burst length. However, in the present model, the length of the burst changes in less intuitive ways. For example, in Fig. 4, we note that the length of the burst *increases* as inhibition is increased from $g_{\text{inh}} = 0.4-0.5$ mS/cm^2, and then decreases in response to further increase in g_{inh}. The initial burst lengthening results from a modulation of the ping-pong interaction between dendrite and soma by inhibition. If inhibition is weak, dendritic voltage is high during the burst leading to fast activation of I_{K-C}, which ends the burst. If inhibition is strong, the dendrite is completely suppressed and does not support a burst of multiple spikes. For intermediate values, the ping-pong effect allows the I_{K-C} current to build up slowly, thereby elongating the burst.

Relation to experimental observations

When synaptic inhibition arrives during a burst, our modeling results suggest that it can modulate the dendritic calcium spike, and thus the somatic firing pattern, in a graded manner. Several experimental studies show complete abolition of dendritic calcium spikes (Buzsáki et al. 1996; Miles et al. 1996; Traub et al. 1994; Tsubokawa and Ross 1996), although an already activated calcium spike could be aborted by inhibition resulting in a shorter calcium spike (Buzsáki et al. 1996). A graded response, however, is suggested by the dendritic recordings of Kamondi et al. (1998) when current pulses of different amplitudes are injected into the dendrite. In their Fig. 7*B*, a strong current pulse evokes a large-amplitude calcium spike. In response to a weaker current pulse, the dendritic voltage displays a group of fast spikes of decrementing ampli-

tude. We compare these results with our model results when no inhibition arrives during the burst and when the dendrite receives a moderate level of inhibition during a burst (Fig. 6*G*). When no inhibition is given, V_d displays a full Ca^{2+}-based spike (1st burst in figure). With moderate inhibition ($g_{inh} = 0.5$ mS/cm^2, 3rd burst in figure), V_d displays a group of back-propagated spikes similar to the initial group of spikes in the Kamondi et al. (1998) dendritic voltage trace. In the Kamondi et al. (1998) trace, the higher frequency of the initial group of spikes, compared to the low-amplitude spikes seen later on during the applied current pulse, seems to suggest a partial depolarization due to dendritic mechanisms that may support somatic spikes in a ping-pong fashion.

In the model, as a result of inhibition arriving during a burst and attenuating the dendritic calcium spike, the following burst was advanced due to less activation of the potassium AHP current. We further found that complex bursts brought on by a distinct dendritic calcium spike occurred at lower frequencies than bursts with fewer number of spikes and that single spikes fired at the highest frequency. A prediction of our modeling results is that, in pyramidal cell firing, bursts consisting of a few spikes will be followed by shorter interburst intervals than bursts consisting of a larger number of spikes. This firing pattern would be a result of less activation of the potassium AHP current with a shorter burst and thus less hyperpolarization of dendritic voltage, leading to crossing of the V_d threshold more quickly. Similarly, the model results predict that single spikes should be followed by the shortest interval to next firing.

In this paper, we have modeled the interneuron as a single cell, and the strength of the synaptic input to the pyramidal cell is determined by the maximal conductance of the synaptic current. As the dendrite compartment represents the lumped distal dendrites of the pyramidal cell, similarly the interneuron could be thought of as representing a pool of interneurons impinging on the distal dendrites, and the maximal conductance could be thought of as a measure of the net inhibitory input. In this way, the model results are not inconsistent with the experimental results that found negligible effect of unitary IPSPs on somatic firing patterns (Karnup and Stelzer 1999; Tsubokawa and Ross 1996). If the single IPSP was received in a background of excitatory input, its effect would not influence the net dendritic depolarization significantly. Our model results suggest that an attenuation of net dendritic depolarization during burst generation may result in modulation of burst waveform.

In this model, the firing frequency and burst waveform observed in the soma compartment were modulated by net dendritic depolarization, which to some extent depended on dendritic calcium concentration. For example, the occurrence of a full dendritic calcium-based spike and the accompanying large increase in intracellular Ca^{2+} resulted in a complex burst in the soma followed by a long interburst interval. But when the dendritic calcium spike was attenuated by inhibition and calcium influx was suppressed, shorter bursts or even single spikes were obtained in the soma and were followed by shorter intervals until the next firing event. These results suggest a dependence of firing pattern and frequency on dendritic calcium concentration, similar to the encoding of firing frequency of cortical layer V pyramidal neurons by dendritic intracellular calcium suggested experimentally (Helmchen et al. 1996) and in models (Wang 1998).

Firing rate changes and phase precession of place cells

Our motivation for studying the effects of synaptic inhibition on pyramidal cell firing is to understand the neural mechanisms responsible for the firing patterns of place cells in hippocampal region CA3. The results presented here suggest that synaptic inhibition may be able to modulate firing rate in a way that is consistent with the experimental observations. Also, the results suggest that firing of the bursting cell can be modulated to produce the phase precession phenomena as modeled in our previous work (Bose et al. 2000). There we proposed that a minimal model consisting of one place cell *P*, one interneuron *I*, and one theta pacemaker *T* could accurately describe the phase precession phenomena. Briefly, we argued that when the animal is outside the place field of the pyramidal cell, the pacemaker drives the interneuron, which in turn entrains the pyramidal cell at the theta rhythm. Within the place field, the pyramidal cell instead drives the interneuron, and they both phase precess relative to the theta pacemaker. The change in control of the interneuron from the pacemaker to the place cell is initiated by the dentate gyrus, which sends an excitatory input to the place cell at the beginning of the place field. The phase precession of *P* and *I* ends after 360° of precession when *I* returns to a phase at which *T* can recapture control of it. Two of the major predictions of that model are that some interneurons phase precess, and that the minimal network could determine the end of the place field with no additional external input. There are two drawbacks of that work, however. One is that within the place field, we only modeled phase and not firing rate. Second, the model predicts an out-of-place field firing rate that is too high. The model presented in this work eliminates both of these concerns. As demonstrated, the interneuron can entrain the pyramidal cell at very low frequencies when the inhibition arrives prior to the burst. This behavior is similar to out-of-place field activity. Additionally, when the pyramidal cell drives the interneuron, the burst frequency is dramatically faster and can exhibit precession. Moreover, changes in firing rate due to changes in the overall level of inhibition versus excitation can be achieved as the animal passes through the place field. For example, a monotonic decrease in the net inhibitory input to a given pyramidal cell would have the effect of increasing its firing rate as seen by Mehta et al. (2000). This decrease could result from added excitation obtained due to recruitment of co-active place cells. The mechanisms for change of control of the interneuron from *T* to *P* and back to *T* remain as before. We shall demonstrate the viability of these ideas in future work.

Our work also can be generalized to show how the same cells can participate in multiple, disjointed place fields. For example, in our two pyramidal cell, one interneuron network, bistability between synchronous and anti-phase or out-of-phase solutions exists. The synchronous solution represents firing of place cells that share the same place field. However, these cells might also be part of other cell assemblies that code for other spatial locations. That the cells can also oscillate out-of-phase, for the same parameter values and synaptic connections, implies that the cells have the potential to participate in multiple cell assemblies. What keeps the cells of different cell assemblies from synchronizing is the level of inhibition versus excitation that any particular cell receives. The analysis of this paper provides a framework to understand the balance between

these two effects. We propose that depending on the timing of the inputs, excitation and inhibition can compete or cooperate to produce multiple types of behaviors.

We thank M. Recce and G. Buzsaki for many helpful discussions.

This research was supported by National Science Foundation Grants IBN-9722946 (to V. Booth) and DMS-9973230 (to V. Booth and A. Bose) and New Jersey Institute of Technology Grants 421590 (to V. Booth) and 421540 (to A. Bose).

REFERENCES

BOSE A, BOOTH V, AND RECCE M. A temporal mechanism for generating the phase precession of hippocampal place cells. *J Comput Neurosci* 9: 5–30, 2000.

BUZSÁKI G, PENTTONEN M, NÁDASDY Z, AND BRAGIN A. Pattern and inhibition-dependent invasion of pyramidal cell dendrites by fast spikes in the hippocampus in vivo. *Proc Natl Acad Sci* 93: 9921–9925, 1996.

CLAIBORNE B, AMARAL D, AND COWAN W. A light and electron microscope analysis of the mossey fibers of the rat dentate gyrus. *J Comp Neurol* 246: 435–458, 1986.

COBB S, BUHL EH, HALASY K, PAULSEN G, AND SOMOGYI P. Synchronization of neuronal activity in hippocampus by individual GABAergic interneurons. *Nature* 378: 75–78, 1995.

CSICSVARI J, HIRASE H, CZURKO A, AND BUZSAKI G. Reliability and state-dependence of pyramidal cell-interneuron synapses in the hippocampus: an ensemble approach in the behaving rat. *Neuron* 21: 179–189, 1998.

FREUND TF AND BUZSÁKI G. Interneurons of the hippocampus. *Hippocampus* 6: 347–470, 1996.

GREEN J AND ARDUINI A. Hippocampal electrical activity in arousal. *J Neurophysiol* 17: 533–557, 1954.

HELMCHEN F, IMOTO K, AND SAKMANN B. Ca^{2+} buffering and action potential–evoked Ca^{2+} signaling in dendrites of pyramidal neurons. *Biophys J* 70: 1069–1081, 1996.

JENSEN O AND LISMAN JE. Hippocampal CA3 region predicts memory sequences: accounting for the phase advance of place cells. *Learn Mem* 3: 257–263, 1996.

JENSEN O AND LISMAN JE. Position reconstruction from an ensemble of hippocampal place cells: contribution of theta phase coding. *J Neurophysiol* 83: 2602–2609, 2000.

KAMONDI A, ACSADY L, WANG X, AND BUZSAKI G. Theta oscillations in somata and dendrites of hippocampal pyramidal cells in vivo: activity-dependent phase-precession of action potentials. *Hippocampus* 8: 244–261, 1998.

KARNUP S AND STELZER A. Temporal overlap of excitatory and inhibitory afferent input in guinea-pig CA1 pyramidal cells. *J Physiol (Lond)* 516: 485–504, 1999.

KEPECS A AND WANG X-J. Analysis of complex bursting in cortical pyramidal neuron models. *Neurocomputing* 32–33: 181–187, 2000.

LARKUM ME, ZHU JJ, AND SAKMANN B. A new cellular mechanism for coupling inputs arriving at different cortical layers. *Nature* 398: 338–341, 1999.

MEHTA MR, QUIRK MC, AND WILSON MA. Experience-dependent asymmetric shape of hippocampal receptive fields. *Neuron* 25: 707–715, 2000.

MILES R, TÓTH K, GULYÁS AI, HÁJOS N, AND FREUND TF. Differences between somatic and dendritic inhibition in the hippocampus. *Neuron* 16: 815–823, 1996.

MORRIS C AND LECAR H. Voltage oscillations in the barnacle giant muscle fiber. *Biophys J* 35: 193–213, 1981.

O'KEEFE J AND BURGESS N. Geometric determinants of the place fields of hippocampal neurons. *Nature* 381: 425–428, 1996.

O'KEEFE J AND DOSTROVSKY J. The hippocampus as a spatial map. Preliminary evidence from unit activity in the freely-moving rat. *Brain Res* 34: 171–175, 1971.

O'KEEFE J AND RECCE ML. Phase relationship between hippocampal place units and the EEG theta rhythm. *Hippocampus* 3: 317–330, 1993.

PINSKY PF AND RINZEL J. Intrinsic and network rhythmogenesis in a reduced Traub model for CA3 neurons. *J Comput Neurosci* 1: 39–60, 1994.

PINSKY PF AND RINZEL J. Erratum. *J Comput Neurosci* 2: 275, 1995.

RUBIN J AND TERMAN D. Geometric analysis of population rhythms in synaptically coupled neuronal networks. *Neural Comp* 12: 597–645, 2000.

SHUTE C AND LEWIS P. Cholinesterase-containing systems of the brain of the rat. *Nature* 199: 1160–1164, 1963.

SKAGGS WE, MCNAUGHTON BL, WILSON MA, AND BARNES CA. Theta-phase precession in hippocampal neuronal populations and the compression of temporal sequences. *Hippocampus* 6: 149–172, 1996.

TERMAN D, BOSE A, AND KOPELL N. Functional reorganization in thalamocortical networks: transition between spindling and delta sleep rhythms. *Proc Natl Acad Sci USA* 93: 15417–15422, 1996.

TERMAN D, KOPELL N, AND BOSE A. Dynamics of two mutually coupled slow inhibitory neurons. *Physica D* 117: 241–275, 1998.

TRAUB R, MILES R, AND JEFFERYS J. Synaptic and intrinsic conductances shape picrotoxin-induced synchronized afterdischarges in the guinea-pig hippocampal slice. *J Physiol (Lond)* 93: 525–547, 1993.

TRAUB RD, JEFFERYS JG, MILES R, WHITTINGTON MA, AND TOTH K. A branching dendritic model of a rodent CA3 pyramidal neurone. *J Physiol (Lond)* 481: 79–95, 1994.

TRAUB RD, WONG R, MILES R, AND MICHELSON H. A model of a CA3 hippocampal pyramidal neuron incorporating voltage-clamp data on intrinsic conductances. *J Neurophysiol* 66: 635–649, 1991.

TSODYKS MV, SKAGGS WE, SEJNOWSKI TJ, AND MCNAUGHTON BL. Population dynamics and theta rhythm phase precession of hippocampal place cell firing: a spiking neuron model. *Hippocampus* 6: 271–280, 1996.

TSUBOKAWA H AND ROSS WN. IPSPs modulate spike backpropagation and associated $[Ca^{2+}]_i$ changes in the dendrites of hippocampal CA1 pyramidal neurons. *J Neurophysiol* 76: 2896–2906, 1996.

VAN VREESWIJK C, ABBOTT L, AND ERMENTROUT GB. When inhibition, not excitation synchronizes neural firing. *J Comp Neurosci* 1: 313–321, 1994.

WALLENSTEIN GV AND HASSELMO ME. GABAergic modulation of hippocampal population activity: sequence learning, place field development, and the phase precession effect. *J Neurophysiol* 78: 393–408, 1997.

WANG XJ. Calcium coding and adaptive temporal computation in cortical pyramidal neurons. *J Neurophysiol* 79: 1549–1566, 1998.

WANG XJ. Fast burst firing and short-term synaptic plasticity: a model of neocortical chattering neurons. *Neuroscience* 89: 347–362, 1999.